

# Ground states in the Many Interacting Worlds approach

Hannes Herrmann\*, Michael J. W. Hall†, Howard M. Wiseman‡, Dirk - André Deckert §

February 17, 2022

## Abstract

Recently the Many-Interacting-Worlds (MIW) approach to a quantum theory without wave functions was proposed. This approach leads quite naturally to numerical integrators of the Schrödinger equation. It has been suggested that such integrators may feature advantages over fixed-grid methods for higher numbers of degrees of freedom. However, as yet, little is known about concrete MIW models for more than one spatial dimension and/or more than one particle. In this work we develop the MIW approach further to treat arbitrary degrees of freedom, and provide a systematic study of a corresponding numerical implementation for computing one-particle ground and excited states in one dimension, and ground states in two spatial dimensions. With this step towards the treatment of higher degrees of freedom we hope to stimulate their further study.

## 1 Introduction

The quantum dynamics of an  $N$ -particle system in  $d$  spatial dimensions is ruled by the Schrödinger equation. The latter defines the evolution of a field  $\Psi$  on the configuration space  $\mathbb{R}^{Nd}$ . A common method to represent such an object numerically is to sample it on a fixed grid. The grid dimensions scale as  $G^{Nd}$ , with  $G$  being the number of grid points along one degree of freedom. This exponential scaling behavior makes integrators based on fixed grids, even on state-of-the-art supercomputers, unfeasible – e.g., settings with  $N = 3$  particles in  $d = 3$  dimensions and a low number of  $G = 10^3$  grid points already require a memory capacity of the order of gigabytes.

Exceptional cases aside, the main two successful general approaches to deal with this quantum complexity problem are as follows. 1) For special initial values and in certain regimes (e.g., product states and high gas densities) one can find approximate solutions by solving non-linear one-particle equations such as the Hartree, Hatree-Fock and Gross-Pitajevski equations; see, e.g., Ref. [1] for an overview. 2) Instead of using a fixed equidistant grid one may employ a

comoving grid that samples the wave functions with high resolution only where it has physically interesting features, while other regions are only covered with very few grid points; see Refs. [2, 3] for an overview. With a well-adapted grid it should in principle be possible to maintain the same accuracy with a significantly lower number of grid-points, especially in long time simulations of, e.g., chemical reaction channels and scattering setups. The approach discussed in this paper belongs to this class 2).

The two central questions in approach 2) are, of course, how to find convenient locations for the grid-points and how to update them in parallel with the evolution of the wave function  $\Psi$  given by the Schrödinger equation:

$$i\partial_t\Psi_t(X) = \hat{H}\Psi_t(X), \quad \hat{H} = -\frac{1}{2}\Delta + V(\hat{X}), \quad (1)$$

for  $t \in \mathbb{R}$  and  $X \in \mathbb{R}^{Nd}$ , where  $\Delta$  denotes the Laplace operator w.r.t.  $X$ ,  $V$  is a classical potential,  $\hat{X}$  is the position operator, and we use units  $t \mapsto t\hbar$  and  $X \mapsto (\hbar/m^{1/2})X$  — we assume here, for simplicity, that all particles have the same mass  $m$ .

One method is to distribute, say  $M$ , grid-points  $Q_{t=0}^{(i)} \in \mathbb{R}^{Nd}$ ,  $i = 1, \dots, M$ , at initial time  $t = 0$  according to the  $|\Psi_{t=0}|^2$ -distribution. Thus, regions with larger contributions to the  $L^2$ -norm are sampled with higher resolution, while regions with smaller contributions are covered only by a few grid points. In order to ensure that the grid points follow the

\*Mathematical Institute, LMU Munich, Germany

†Centre for Quantum Dynamics, Griffith University, Brisbane, QLD 4111, Australia

‡Centre for Quantum Dynamics, Griffith University, Brisbane, QLD 4111, Australia

§Mathematical Institute, LMU Munich, Germany

$|\Psi_t|^2$ -distribution (a feature usually referred to as equivariance in the context of Bohmian mechanics) [5] one must transport them along the flux lines of the quantum probability current [4], i.e., along Bohmian trajectories  $Q_t^{(i)}$  which obey the Bohmian law of motion [5]

$$\frac{dQ_t^{(i)}}{dt} = \Im \frac{\Psi_t^*(X) \cdot \nabla \Psi_t(X)}{\Psi_t^*(X) \cdot \Psi_t(X)} \Big|_{X=Q_t^{(i)}}. \quad (2)$$

This means that one needs to integrate Bohm's velocity law (2) simultaneously with the Schrödinger equation (1) on comoving coordinates  $Q_t^{(i)}$ ,  $i = 1, \dots, M$  to track the Schrödinger evolution. Using the decomposition  $\Psi_t = \sqrt{P_t} e^{iS_t}$ , the corresponding coupled set of equations (1)-(2) in comoving coordinates takes the form [2]:

$$\frac{d}{dt} P_t(Q_t^{(i)}) = -P_t(Q_t^{(i)}) \Delta S_t(Q_t^{(i)}) \quad (3)$$

$$\frac{d}{dt} S_t(Q_t^{(i)}) = \frac{1}{2} \left( \frac{d}{dt} Q_t^{(i)} \right)^2 - V(Q_t^{(i)}) - U_t(Q_t^{(i)}) \quad (4)$$

$$\frac{d^2}{dt^2} Q_t^{(i)} = -\nabla V(Q_t^{(i)}) - \nabla U_t(Q_t^{(i)}) \quad (5)$$

for initial value constraint

$$\frac{d}{dt} Q_t^{(i)}|_{t=0} = \nabla S_t(Q_t^{(i)})|_{t=0} \quad (6)$$

and quantum potential

$$U_t(X) = -\frac{1}{2} \frac{\Delta P_t(X)^{1/2}}{P_t(X)^{1/2}}. \quad (7)$$

Note that constraint (6) together with (5) is equivalent to (2), in view of the corresponding initial value problem, while thanks to (7), (3)-(4) are equivalent to (1). Numerical analysis of quantum systems with the help of trajectories has been studied in great depth and we refer the reader to the literature, e.g., [2, 3, 6, 7].

A further simplification can be attained when not only the grid points are distributed randomly according to  $|\Psi|^2$  but when the  $|\Psi|^2$ -distribution itself can be approximately retrieved from the empirical distribution of the grid point locations  $Q_t^{(i)}$ , via some map  $P(X; Q_t^{(1)}, \dots, Q_t^{(M)})$  such that for all  $t, X$  the approximation

$$P_t(X) \approx P(X; \mathcal{Q}_t), \quad \mathcal{Q}_t := (Q_t^{(1)}, \dots, Q_t^{(M)}) \quad (8)$$

holds in a suitable sense as  $M \rightarrow \infty$ . In view of the weak law of large numbers, one may think of

$P(X; \mathcal{Q}_t)$  as a smooth version of the empirical distribution

$$P(X; \mathcal{Q}_t) \approx \frac{1}{M} \sum_{i=1}^M \delta^{Nd}(X - Q_t^{(i)}), \quad (9)$$

as the  $Q_t^{(i)}$ ,  $i = 1, \dots, M$ , stay approximately  $|\Psi_t|^2$  distributed thanks to equivariance. Once a good candidate for  $P(X; \mathcal{Q}_t)$  and its derivatives is identified, equations (3)-(6) can be replaced by a closed set of equations for the trajectories  $Q_t^{(i)}$ . It suffices, for example, to only solve the system of equations

$$\frac{d^2}{dt^2} Q_t^{(i)} = -\nabla [V(X) + U(X; \mathcal{Q}_t)] \Big|_{X=Q_t^{(i)}} \quad (10)$$

under the initial constraint (6), where now the density  $P_t(X)$  in the quantum potential (7) is replaced by  $P(X; \mathcal{Q}_t)$  so that the approximate quantum potential reads

$$U(X; \mathcal{Q}_t) = -\frac{1}{2} \frac{\Delta P(X; \mathcal{Q}_t)^{1/2}}{P(X; \mathcal{Q}_t)^{1/2}}. \quad (11)$$

Quantum expectation values of an observable  $f(\hat{X})$  can now be recovered simply from the trajectories  $Q_t^{(i)}$  by

$$\begin{aligned} \langle \Psi_t, f(\hat{X}) \Psi_t \rangle &= \int d^{Nd} X P_t(X) f(X) \\ &\approx \int d^{Nd} X P(X; \mathcal{Q}_t) f(X) \\ &\approx M^{-1} \sum_{i=1}^M f(Q_t^{(i)}). \end{aligned} \quad (12)$$

Several discrete and continuous versions of this approach have been proposed in the literature [8–15]. Due the possible interpretation of  $Q_t^{(i)}$ ,  $i = 1, \dots, M$ , as  $M$  coexisting “worlds” we follow Ref. [12] in referring to this approach as the Many-Interacting-Worlds (MIW) approach.

The MIW approach stands or falls according to the possibility of finding a good candidate  $P(X; \mathcal{Q}_t)$  and the ability to maintain the quality of the approximation (8) over time for  $M$  not too large. In Ref. [12] we have presented a surprisingly simple toy model for  $N = 1$  particle in  $d = 1$  dimension with the ansatz

$$\begin{aligned} &P(Q^{(i)}; \mathcal{Q}_t) \\ &:= \frac{1}{2} \left( \frac{1}{N(Q^{(i)} - Q^{(i-1)})} + \frac{1}{N(Q^{(i+1)} - Q^{(i)})} \right) \end{aligned} \quad (13)$$

for  $i = 1, \dots, M$ , with the ordering  $Q_0^{(i)} < Q_0^{(i+1)}$  (setting  $Q_t^{(0)} = -\infty, Q_t^{(M+1)} = +\infty$ ). The above ordering is preserved over time because the system (1)

and (5) has a well-defined initial value problem [16], and hence, configuration space trajectories cannot cross. However, instead of approximating  $U_t(X)$  directly via a smoothed  $P(X; \mathcal{Q}_t)$ , as in Eq. (11), the method in Ref. [12] approximates its average (proportional to the Fisher information of  $P_t(X)$ ), via

$$\begin{aligned} \bar{U}_t &= \int d^{Nd} dX P_t(X) U_t(X) \\ &= \frac{1}{8} \int P_t(X) \left| \frac{\nabla P_t(X)}{P_t(X)} \right|^2 \\ &\approx \frac{1}{8} \sum_{i=1}^M \left| \frac{\nabla P(Q^{(i)}; \mathcal{Q}_t)}{P(Q^{(i)}; \mathcal{Q}_t)} \right|^2. \end{aligned} \quad (14)$$

Using Eq. (13) and the corresponding discrete approximation of  $\nabla P_t(X)$  for  $N = d = 1$ , this leads to the replacement of Eq. (10) by the very similar form

$$\frac{d^2}{dt^2} Q_t^{(i)} = -\nabla_{Q_t^{(i)}} \left[ V(Q_t^{(i)}) + U^{\text{MIW}}(\mathcal{Q}_t) \right], \quad (15)$$

where

$$\begin{aligned} U^{\text{MIW}}(\mathcal{Q}_t) &= \\ &= \frac{1}{8} \sum_{i=1}^M \left( \frac{1}{Q^{(i+1)} - Q^{(i)}} - \frac{1}{Q^{(i)} - Q^{(i-1)}} \right)^2. \end{aligned} \quad (16)$$

The resulting model defined by Eqs. (15) and (16) has the nice property of conserving the total energy [12]

$$E = \sum_{i=1}^M \left[ \frac{1}{2} \left( \frac{dQ_t^{(i)}}{dt} \right)^2 + V(Q_t^{(i)}) \right] + U^{\text{MIW}}(\mathcal{Q}_t), \quad (17)$$

and will be referred to as the 1d MIW model throughout this work.

In Ref. [12], the 1d MIW model was shown to exhibit typical quantum behavior such as superposition and tunneling. In particular, numerical implementation of the model, with a very modest number of worlds, gave good qualitative agreement in the case of the time-evolution of two superposed Gaussians (representing double-slit interference). In addition, numerical testing showed good quantitative agreement for the computation of ground states, and convergence in the limit  $M \rightarrow \infty$  has been proven for a harmonic potential [17].

The goal of this paper is to develop the MIW approach further, to treat more than one degree of freedom. Section 2 provides a general model for any finite number of degrees of freedom, i.e., finite particle numbers and spatial dimensions. In the spirit of

this general approach we then present numerical algorithms for finding energy eigenstates. First, we consider the 1d case in section 3.2, to benchmark our new method against the original 1d MIW model, using the harmonic and the Pöschl-Teller potentials, and we present results for both ground and excited states. Second, we generalize our method of finding ground states to  $d = 2$  dimensions in section 3.4. In particular, we discuss our numerical results again for the harmonic and Pöschl-Teller potentials. In comparison to the harmonic potential, the Pöschl-Teller potential is only weakly confining, which makes the lack of information at spatial infinity much more prominent in numerical simulations. We discuss how this problem can be successfully addressed in our approach.

The numerical methods and simulations reported here are based on results in [18]. Independent calculations have been made very recently by Sturniolo [19], for the ground states of higher dimensional systems in the framework of the MIW approach, which we comment on briefly in section 4.

## 2 Generalization to arbitrarily many degrees of freedom

A formal extension of the 1d MIW model, to a system of  $N$  particles moving in  $d$  spatial dimensions, is given by retaining the equations of motion, Eq. (15), but generalizing Eq. (16) to

$$U^{\text{MIW}}(\mathcal{Q}_t) = \frac{1}{8} \sum_{i=1}^M \left| \frac{\nabla P(Q_t^{(i)}; \mathcal{Q}_t)}{P(Q_t^{(i)}; \mathcal{Q}_t)} \right|^2, \quad (18)$$

for suitable approximations  $P(Q_t^{(i)}; \mathcal{Q}_t)$  and  $\nabla P(Q_t^{(i)}; \mathcal{Q}_t)$ , of  $P_t(Q_t^{(i)})$  and its derivative, respectively [12]. We now show how to construct these two approximations in turn.

### 2.1 Approximating the probability density

We will consider two related approaches here, based on triangulation and cells, respectively.

#### 2.1.1 Triangulation method

The worlds or trajectories  $Q_t^{(i)}$  lie in the  $D$ -dimensional configuration space  $\mathbb{R}^{Nd}$  with  $D := Nd$ . This configuration space can be partitioned into a network of  $D$ -tetrahedra having the worlds as vertices, together with a single exterior region. For  $D = 2$  this corresponds to a triangulation of the configuration space, together with an exterior region.

Such a triangulation is depicted in the left hand panel of figure 1 (purple lines), corresponding to a Delaunay triangulation [24]. Efficient algorithms are known for establishing such triangulations [24].

For a given triangulation, let  $\{T_{i,j}\}$  denote the set of  $D$ -tetrahedra (“triangles”) sharing  $Q^{(i)}$  as a common vertex, at a given time  $t$ . Here we have dropped the explicit time label on  $Q^{(i)}$  for convenience. Now, for a sufficiently smooth function  $f(X)$  on configuration space one can, similarly to Eq. (12), approximate its average via

$$\begin{aligned} \frac{1}{M} \sum_{i=1}^M f(Q^{(i)}) &\approx \int dX P(X) f(X) \\ &= \frac{1}{D+1} \sum_{i,j} \int_{T_{i,j}} dX P(X) f(X) \\ &\approx \frac{1}{D+1} \sum_{i,j} |T_{i,j}| P(Q^{(i)}) f(Q^{(i)}), \end{aligned} \quad (19)$$

where  $|T_{i,j}|$  denotes the volume of the tetradron  $T_{i,j}$ , and the factor of  $D+1$  arises because every tetrahedron is counted once for each of its  $D+1$  vertices. Hence, equating these expressions for arbitrary  $f(X)$ , a suitable approximation for the probability density at  $Q^{(i)}$  is given by

$$P_{\text{tri}}(Q^{(i)}; \mathcal{Q}) = \frac{D+1}{M \sum_j |T_{i,j}|}. \quad (20)$$

This reduces to Eq. (13) for the 1d MIW model when  $D = Nd = 1$ .

### 2.1.2 Cell method

An alternative to placing worlds at the vertices of a triangulation is to instead place each world within an individual cell, where the cells partition the configuration space. For example, for a Delaunay triangulation such cells can be chosen as the dual graph, corresponding to Voronoi cells [24]. An example is depicted in the right panel of figure 1. Note that some cells, corresponding to worlds at the edges, are infinite in extent.

Such a partitioning leads to the alternative approximation

$$P_{\text{cell}}(Q^{(i)}; \mathcal{Q}) = \frac{1}{M |\text{Cell}_i|} \quad (21)$$

for the probability density at  $Q^{(i)}$ , where  $|\text{Cell}_i|$  denotes the configuration space volume of the cell containing trajectory  $Q^{(i)}$ .

## 2.2 Approximating the derivative of the probability density

Equation (18) further requires finding a suitable approximation for the derivative  $\nabla P(Q^{(i)})$  at each time (where again we suppress the explicit dependence on time for convenience). This derivative has  $D = Nd$  independent components, and hence we need to consider, for each trajectory  $Q^{(i)}$  at that time, the change in probability in at least  $D$  different directions. These directions could be chosen, for example, to be those which join  $Q^{(i)}$  to its  $D$  closest neighbours, independently of the method used to estimate the density itself (e.g., via triangulation or cells). An alternative choice is to use the directions corresponding to all (or some) edges of a given triangulation which have  $Q^{(i)}$  as a vertex. Yet another choice is to use the directions corresponding to all (or some) worlds that share a cell boundary with  $Q^{(i)}$ .

Here we will be quite general, and only suppose that  $C_i \geq D$  neighbouring configurations or worlds are used to estimate  $\nabla P(Q^{(i)})$ , where these may be selected by any of the means above. Let  $\{Q^{(i,s)}\}$  denote these  $C_i$  configurations, and define the corresponding set of vectors

$$v^{(i,s)} := Q^{(i,s)} - Q^{(i)}. \quad (22)$$

By construction, these form a (typically overcomplete) basis set in configuration space. Now, writing

$$v^{(i,s)} = \sum_{k=1}^D A_{sk} e_k \quad (23)$$

relative to some orthonormal basis set  $\{e_k\}$ , one has a corresponding set of dual basis vectors  $\tilde{v}^{(i,s)} := \sum_k \tilde{A}_{sk} e_k$ , with  $\tilde{A} := A(A^\top A)^{-1}$ . This dual basis satisfies the completeness property

$$\sum_s \tilde{v}^{(i,s)} (v^{(i,s)})^\top = I_D, \quad (24)$$

where  $\top$  denotes the transpose and  $I_D$  is the  $D \times D$  identity matrix. Using  $P(Q^{(i,s)}) - P(Q^{(i)}) \approx v^{(i,s)} \cdot \nabla P(Q^{(i)})$ , it follows immediately that one has

$$\begin{aligned} \nabla P(Q^{(i)}) &= \sum_s \tilde{v}^{(i,s)} (v^{(i,s)})^\top \nabla P(Q^{(i)}) \\ &\approx \sum_s \left[ P(Q^{(i,s)}) - P(Q^{(i)}) \right] \tilde{v}^{(i,s)}. \end{aligned} \quad (25)$$

For any suitable approximation of  $P(Q^{(i)}; \mathcal{Q})$ , such as in Eqs. (20) or (21), one then has the corresponding approximation

$$\nabla P(Q^{(i)}; \mathcal{Q}) = \sum_s \left[ P(Q^{(i,s)}; \mathcal{Q}) - P(Q^{(i)}; \mathcal{Q}) \right] \tilde{v}^{(i,s)} \quad (26)$$

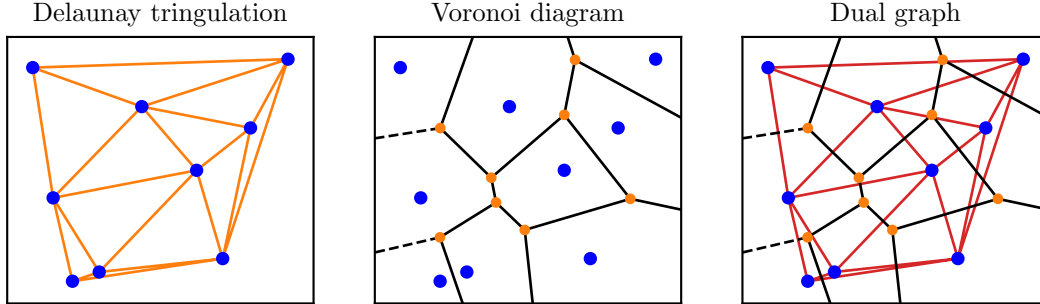


Figure 1: The left hand panel shows a Delaunay triangulation of configuration space for a set of worlds (blue circles) at a given time. Each triangle (orange edges) is chosen in such a way that no worlds lie inside the circum-sphere of any triangle. The middle panel shows its dual graph, corresponding to partitioning configuration space into Voronoi cells (see definition (37) below). The corresponding cell boundaries are formed by hyperplanes (black lines) which bisect the triangulation lines. The right panel illustrates the duality of these graphs.

of the derivative. This may be inserted into Eq. (18) to obtain the corresponding MIW potential function  $U^{\text{MIW}}(Q_t)$  at any given time  $t$ .

### 3 A numerical implementation for ground states

Following the spirit of the general approach in section 2 we will now provide numerical implementations in 1d and 2d which are based on the work in Ref. [18]. We will concentrate primarily on the numerical determination of ground state energies and distributions, although we do also consider excited states in the 1d case.

While the approach given in section 2 is precise and general, we encountered several problems in its direct numerical implementation. For example, the construction of the dual basis set  $\{\tilde{v}^{(i,s)}\}$  appearing in Eq. (26) requires computation of the inverse of the  $C_i \times C_i$  matrix  $(A^\top A)^{-1}$  for each of the  $M$  worlds. Recalling that  $C_i \geq D = Nd$ , this alone requires  $O(MN^3d^3)$  calculations at each time step. Moreover, unlike the one-dimensional case, the set of neighboring configurations or worlds used to define triangulations, partitionings, derivatives, etc., can change over time, and thus requires constant updating.

These problems originate from the use of neighboring worlds for obtaining approximations of  $P_t(X)$  and its derivative at a given world  $Q_t^{(i)}$ . The selection of finitely many nearest neighbors inevitably provokes discontinuous changes throughout the dynamics. Though for very large  $M$  one may expect that

these sudden jumps may have only have little impact on the overall dynamics of worlds, this is not the case for lower values of  $M$ . There, these small discontinuities may cause oscillations in the world configurations  $Q_t^{(i)}$  which are not damped, and which propagate through the whole system until the numerical simulation breaks down. This forced us to replace this discrete notion of nearest neighbors, in computing the approximate  $P_t(X)$  and its derivatives, by something more smooth.

It turns out that finding a smooth distribution that approximates the empirical distribution is an old problem, discussed thoroughly in the classical literature; see [20–23] for an overview. One general and, for many settings, very robust technique is so-called smooth kernel density estimation, which we introduce first.

The density estimator for a given distribution of worlds  $\mathcal{Q} = (Q^{(1)}, \dots, Q^{(M)})$  is given by a sum of the form

$$P_h(X; \mathcal{Q}) := \frac{1}{\tilde{M}} \sum_{i=1}^{\tilde{M}} \frac{1}{h_i} K\left(\frac{X - \tilde{Q}^{(i)}}{h_i}\right). \quad (27)$$

Here  $\{\tilde{Q}^{(i)}\}$  is a set of  $\tilde{M}$  points in configuration space determined by  $\mathcal{Q}$ ; the  $h_i$  are width parameters (usually referred to as bandwidths) similarly determined by  $\mathcal{Q}$ ; and  $K$  is a smooth kernel function that fulfills  $\int d^{Nd}X K(X) = 1$ . Note that  $P_h(X; \mathcal{Q})$  is automatically normalized. Although, this leaves a lot of freedom, in this work we will only focus on the Gaussian kernel  $K(X) = (2\pi)^{-Nd/2} \exp(-\frac{1}{2}X^\top X)$ , for which  $\tilde{Q}^{(i)}$  takes the role of a mean and  $h_i^2 I_{Nd}$  defines a corresponding covariance matrix (we do not explore

more general covariance matrices here). Considering that the Schrödinger propagator is given by a Gaussian [5], this seems like a canonical choice.

The idea behind ansatz (27) is to allow for varying widths  $h_i$ , well-adapted to regions of high and low empirical density in the vicinity of conveniently chosen locations  $\tilde{Q}^{(i)}$ . If the empirical density is low in the neighborhood of  $\tilde{Q}^{(i)}$ , one chooses large values of  $h_i$ , i.e., broad kernel functions, and if the density is high, one chooses small values, i.e., peaked kernel functions. We will come back to the question of choosing optimal  $\tilde{Q}^{(i)}$  and  $h_i$  later, in sections 3.2 and 3.4. We first show how density estimation may be used in an algorithm for calculating ground state properties.

### 3.1 Gaussian kernel algorithm

Once the choice for the  $\tilde{Q}^{(i)}$  and  $h_i$  is settled, an algorithm for finding ground states can be given in terms of the following iteration:

1. Start with any initial distribution of  $M$  worlds  $\mathcal{Q}_0 = \{Q_0^{(1)}, \dots, Q_0^{(M)}\}$  and choose a suitably small time step  $\Delta t > 0$ .
2. From  $\mathcal{Q}_0$ , compute the approximate potential (11) in which the approximate density  $P(X; \mathcal{Q}_t)$  is replaced by  $P_h(X; \mathcal{Q}_0)$  given in (27).
3. Integrate the second order equation of motion (10) up to time  $\Delta t$  with zero initial velocities  $\dot{Q}_0^{(i)} = 0$ , to obtain a new empirical distribution  $\mathcal{Q}_{\Delta t}$ .
4. Replace  $\mathcal{Q}_0$  by  $\mathcal{Q}_{\Delta t}$  and go back to step 2 until a predefined stopping condition is met (e.g. given by an appropriate measure of convergence).

We shall refer to this algorithm as the *Gaussian kernel algorithm*.

A similar algorithm was discussed for the 1d MIW model in Ref. [12]. The reason why convergence can be expected is that in every integration step of (10) the initial velocities are set to zero. This introduces a loss of energy, as after each integration step 3 above the total energy

$$E_{\text{kin}}(\Delta t) + E_{\text{pot}}(\Delta t) = \sum_{i=1}^M \left[ \frac{1}{2} \left( \dot{Q}_{\Delta t}^{(i)} \right)^2 - \int_0^{\Delta t} ds \dot{Q}_s^{(i)} \cdot \nabla [V(X) + U(X; \mathcal{Q}_s)]_{X=Q_s^{(i)}} \right] \quad (28)$$

is reduced by the positive kinetic energy  $E_{\text{kin}}$ . Hence, during the iteration of the algorithm the configuration of worlds  $\mathcal{Q}$  will arrange itself to find a local minimum of  $E_{\text{pot}}(\Delta t)$ . Providing that the potential  $V(X)$

is confining, e.g., as in the case of a harmonic potential, it will work to focus the worlds, while the potential  $U(X; \mathcal{Q})$  will work against clustering of worlds (cf. Ref. [12]). Since the integration time step  $\Delta t$  is small, and near a local minimum the velocities  $\dot{Q}_s^{(i)}$  in Eq. (28) can also be expected to be small, a local minimum of  $E_{\text{pot}}$  should then fulfill

$$\nabla [V(X) + U(X; \mathcal{Q})]_{X=Q^{(i)}} \approx 0, \quad (29)$$

which according to the Bohmian equation of motion corresponds to a stationary state [5]. If  $V(X)$  has only one local minimum one can, therefore, expect that the algorithm converges to a configuration of worlds  $\mathcal{Q}$  that is distributed according to  $|\Psi|^2$ , where  $\Psi$  is the ground state of the system with Hamiltonian  $\hat{H}$  as per (1).

The main difference between the above algorithm, employing Gaussian kernels, and the MIW algorithm given in Ref. [12], is that the latter does not use a density estimator but instead computes forces as per (15), using the MIW potential (16), where the latter is conservative as per Eq. (17). One of the advantages of the Gaussian kernel model introduced here is that its form readily generalizes to any number of degrees of freedom  $Nd$  without sacrificing smoothness. In contrast, the form of (15) and its generalization via Eq. (18) depend on the use discrete derivatives, defined via finitely many neighbouring worlds, which leads to continuity issues as discussed at the beginning of this section.

### 3.2 Application to 1d ground states

The goal of this section is to provide a numerical implementation of the Gaussian kernel algorithm for  $Nd = 1$ . This allows a comparison with the MIW algorithm studied in Ref. [12], and will provide the basis for the generalization to  $Nd = 2$  in section 3.4.

The first question we must address is the choice of the  $\tilde{Q}^{(i)}$  and  $h_i$  in Eq. (27), on which the performance of the algorithm will crucially depend. Several explicit forms for  $\tilde{Q}^{(i)}$  and  $h_i$  have been considered in the literature on kernel density estimators, for various situations. For example, Ref. [21] discusses an explicit dependence of  $h_i$  on the  $k$ -th nearest neighbors distance w.r.t.  $\tilde{Q}^{(i)} = Q^{(i)}$ . However, for reasons discussed above, we want to avoid a dependence on discontinuous quantities such as the nearest neighbor distance, as much as possible. Hence we propose another approach here.

For the case  $Nd = 1$  (although not for higher values), it is important to observe that the world configurations  $\mathcal{Q}_{\Delta t}^{(i)}$  found in step 3 of the Gaussian ker-

nel algorithm in Sec. 3.1 should be good approximations to Bohmian trajectories, and as such may not cross [4]. In particular, if a crossing occurs then the trajectories  $Q_{\Delta t}^{(i)}$  are no longer trustworthy, and there is no reason why in future iterations of the algorithm they will converge to a sensible distribution. However, for very large  $M$ , crossings may easily occur due to numerical errors. Hence, for  $Nd = 1$  it is important to implement a mechanism that effectively works against such catastrophic crossing events. We note that such events are much more suppressed in the 1d MIW model, due to the singular repulsion between neighbouring worlds [12].

One mechanism that we found to work well is implemented by choosing the  $\tilde{Q}^{(i)}$  to be located midway between the actual world configurations  $Q^{(i)}$ :

$$\tilde{Q}^{(i)} := \frac{1}{2}(Q^{(i)} + Q^{(i+1)}), \quad (30)$$

for  $i = 1, \dots, \tilde{M} = M - 1$ . Provided the width parameters  $h_i$  are set appropriately, this choice induces a peak in the density  $P_h(X; \mathcal{Q})$  to build up between any two approaching worlds  $Q_{\Delta t}^{(i)}$  and  $Q_{\Delta t}^{(i+1)}$ . By virtue of the second derivative (11) the corresponding quantum force on the right-hand side of (10) then acts to repel these two approaching worlds; *cf.* Ref. [4].

In order to determine good bandwidths  $h_i$  we constrain the estimator ansatz (27) by

$$P_h(\tilde{Q}^{(i)}; \mathcal{Q}) \stackrel{!}{=} \frac{1}{M+1} \frac{1}{Q^{(i+1)} - Q^{(i)}} =: p_i \quad (31)$$

for all  $i = 1, \dots, M - 1$ . The a priori estimate of the density  $p_i$  between the two worlds is, of course, very much related to the a priori density that was used to construct the MIW model; *cf.* (13). This formula stems from the mean value theorem and can be seen as special case of (21). Instead of trying to infer an analytic solution for this constraint (which may not be possible in general), we implement the recursion relation

$$h_i \leftarrow h_i \frac{P_h(\tilde{Q}^{(i)}; \mathcal{Q})}{p_i}, \quad (32)$$

which in typical situations considered in this paper gives good results after just a few iterations. Figure 2 illustrates the density estimation in two cases (see the figure caption for further discussion).

For the numerical implementation of the Gaussian kernel algorithm we chose a similar setting as for the MIW algorithm discussed in Ref. [12]:  $V(X) = \frac{1}{2}\hbar^2\omega^2 X^2$  for magnitude of  $\hbar^2\omega^2$  being one,  $M = 20$  worlds, and a time step of  $\Delta t = 4.9 \cdot 10^{-5} s^{-1} \hbar$  over  $10^5$  iterations. The convergence of the configuration

of worlds  $\mathcal{Q}$  is illustrated in the top panel of figure 3, with the corresponding result for the MIW algorithm shown in the bottom panel for comparison. As a measure of the performance and accuracy of the algorithms we used the convergence of ground state energy which is illustrated in figure 4. The 1d MIW model algorithm was already shown [12] to converge to a ground state energy of  $\frac{1}{2}(1 - M^{-1})$ , corresponding to an asymptotic relative error of  $M^{-1} = 5 \cdot 10^{-2}$ , as depicted in the right panel of the figure. In contrast, the Gaussian kernel algorithm gives a smaller (albeit oscillating) relative error as can be seen in figure 4. Whereas the MIW algorithm systematically underestimates the ground state energy as above, the Gaussian kernel algorithm appears to systematically overestimate the energy. Furthermore, the Gaussian kernel algorithm converges rather faster to the ground state distribution. This behavior is very likely due to the fact that the Gaussian kernel function are well adapted to the approximate the ground state density for a harmonic potential. Overall, in [18], the Gaussian kernel algorithm was tested in various scenarios (and for different potentials) and performed quite robustly in approximating the respective ground states.

### 3.3 Extension to 1d excited states

We observed the above algorithm to also converge quickly for various other potentials. Hence, a next natural question is if one can also find excited states by a similar approach. After all, for excited states one would similarly have to look for a distribution of worlds such that (29) is fulfilled. However, we found that this does not work out-of-the-box. One reason is that, according to the Gaussian kernel algorithm introduced above, the energy of the configuration of worlds is monotonically decreasing in integration time. Any numerical inaccuracy in the configuration of worlds approximating the distributed of square modulus of an excited wave function (which for  $N < \infty$  is generic) may likely cause the energy to decrease below the one of the excited states in the next integration step, after which the energy will decrease further until a ground state configuration is approached. To find a particular excited state one must therefore search for a ground state w.r.t. a Hilbert space that excludes the span of all eigenstates below a certain energy level.

An intuition for how to implement such a restriction comes from Courant's old observation [26] that (assuming a sufficiently regular potential) the number of nodes of the wave function of the  $n$ -th excited state is divided in no more than  $n$  subdomains of the configuration space, and in particular, the ground

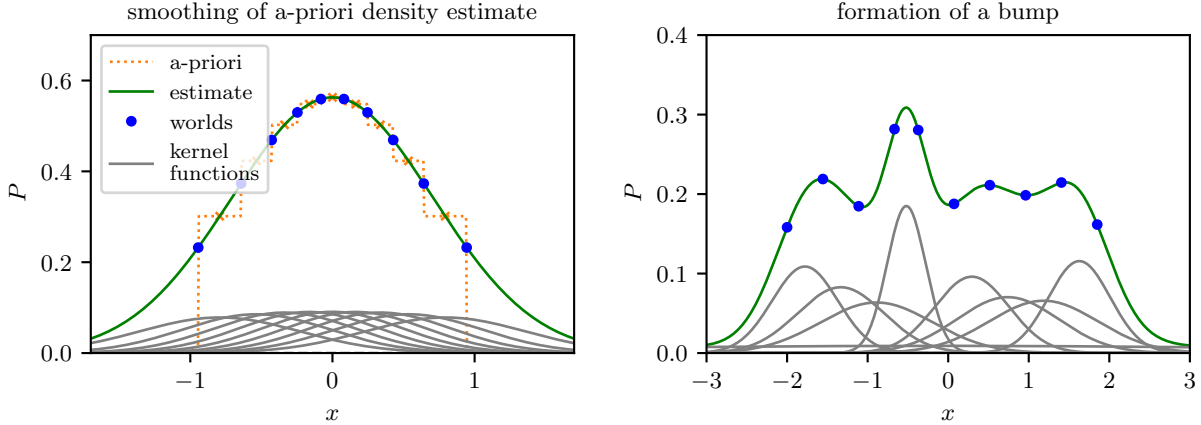


Figure 2: The left panel illustrates 1d kernel density estimation, as per Eqs. (27), (30) and (31), for the case of a Gaussian distributed configuration of worlds  $\mathcal{Q}$ . The  $M = 10$  worlds  $Q^{(i)}$  are shown as red dots, the  $\tilde{M} = 9$  midpoints  $\tilde{Q}^{(i)}$  in Eq. (30) correspond to the blue crosses, and the *a priori* density estimates  $p_i$  are plotted as the blue dotted line. The corresponding Gaussian kernels are shown in gray, and sum to  $P_h(X; \mathcal{Q})$  (depicted by the green curve) as per Eq. (27). The right panel shows how the density estimate naturally develops a bump between two nearby worlds (see also Sec. 3.2).

state does not admit any nodes; see [27] for a modern discussion. Exploiting this observation, we may restrict the search for a stationary with a certain pre-determined number of nodes by replacing our density estimator (27) by a new one that imposes the nodes manually:

$$ZP_h(X; \mathcal{Q}) := \sum_{i=1}^{\tilde{M}} \frac{1}{h_i} K\left(\frac{X - \tilde{Q}^{(i)}}{h_i}\right) - \sum_{i=1}^{\tilde{M}} \frac{1}{\bar{h}_i} K\left(\frac{X - \bar{Q}^{(i)}}{\bar{h}_i}\right). \quad (33)$$

Here,  $\bar{M}$  denotes the number of enforced nodes and  $\bar{Q}^{(i)}$  their positions. Note the minus sign in front of the second summand and the normalization constant  $Z$  on the left-hand side. The additional parameters  $\bar{h}_i$  play the same role as the  $h_i$  and determine the behavior of the world distribution near a node. Unfortunately, this new density estimator may assume negative values and therefore may in general not give rise to a proper probability density. However, in our first trials with the harmonic and Pöschl-Teller potential this fact has turned out to be negligible for the performance of the algorithm.

In 1d using the Gaussian kernel algorithm as described above, it turns out to be sufficient to work with the old density estimator (27) for the same  $\tilde{M}$  while allowing for negative  $h_i$  (since the kernels are symmetric). Instead of enforcing the nodes at the

level of the density estimator as was done in (33) they can be enforced by changing the *a priori* estimate (31) into

$$P_h(\tilde{Q}^{(i)}; \mathcal{Q}) \stackrel{!}{=} \frac{1}{M+1} \frac{1}{Q^{(i+1)} - Q^{(i)}} \chi_i, \quad (34)$$

where  $\chi_i = 0$  if there is supposed to be a node between worlds  $\tilde{Q}^{(i)}$  and  $\tilde{Q}^{(i+1)}$ , while otherwise  $\chi_i = 1$ . The recursion (32) must also be changed, in order to allow for vanishing right-hand side of (31). One possible choice is given by

$$h_i \leftarrow \frac{K(0)}{p_i - P_h(\tilde{Q}^{(i)}; \mathcal{Q}) + h_i^{-1} K(0)}. \quad (35)$$

In [18] several choices (including the above) have been numerically studied and benchmarked. Here we give the results found for the harmonic potential  $V(X) = \frac{1}{2} \hbar^2 \omega^2 X^2$  and the Pöschl-Teller potential  $V(X) = \frac{\alpha^2}{2} \frac{\lambda(\lambda+1)}{\cosh^2(\alpha X)}$ , for which we chose  $\lambda = 6$ ; see figure 5. For both potentials we have set up the Gaussian kernel algorithm to find the first excited ground state. This was done by exploiting the radial symmetry of the potentials which dictates that one node has to be enforced at the origin. For both cases we found a fairly quick convergence up to an accuracy that is of the same order of magnitude as the one found in the computation of the ground states (see figure 4). After this convergence phase the computed energy values starts to oscillate with high frequency but small



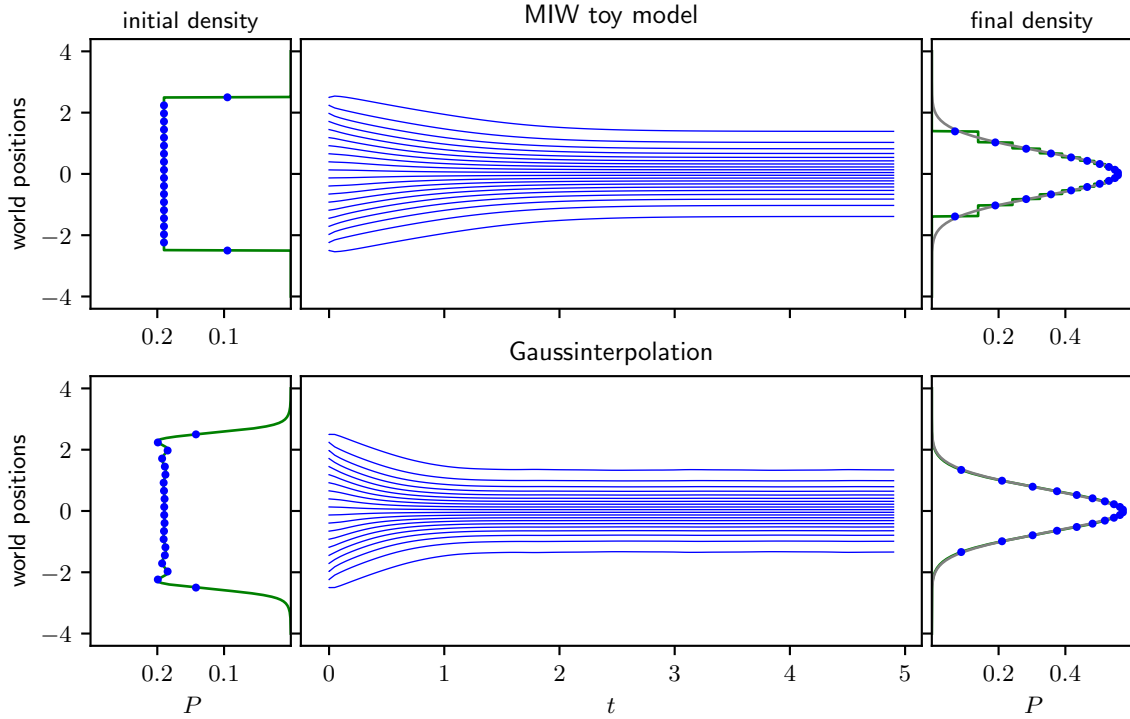


Figure 3: Comparison of the convergence of the Gaussian kernel algorithm (top panel) and the MIW algorithm (bottom panel) in the case of a 1d harmonic potential  $V(X) = \frac{1}{2}\hbar^2\omega^2 X^2$ ,  $M = 20$  worlds, and  $\Delta t = 4.9 \cdot 10^{-5}$  in units of  $\hbar$  over  $10^5$  iterations (see also Sec. 3.2). The two plots on the left illustrate the initial spacing of the worlds  $\mathcal{Q}$ , which was chosen to be uniform (blue dots), and the density estimate using (27) and (32) respectively (green curves). The two middle plots show the evolving configuration of the worlds during the iteration of the algorithms and the plots on the right show the final densities after the convergence.

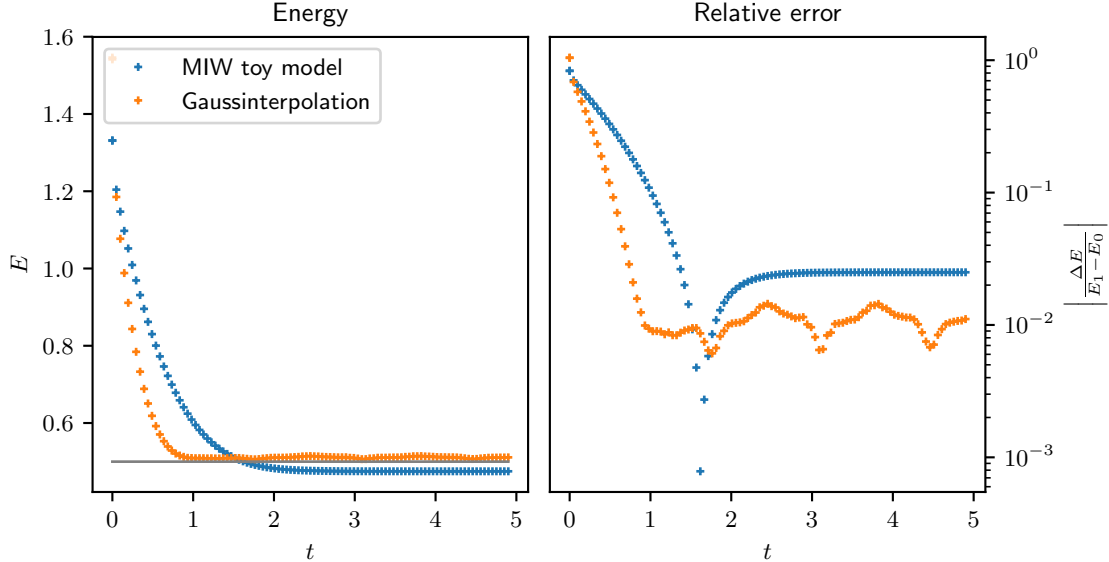


Figure 4: Convergence of the total energy and the relative error for the Gaussian kernel algorithm (blue + markers) and the 1d MIW model algorithm (orange + markers), for the same setting as in figure 3 (see also Sec. 3.2). The energy is plotted in units of  $\hbar\omega$ . The relative error is given as difference w.r.t. the true ground state and normalized w.r.t. the energy difference between the first excited and ground state energy, i.e.,  $E_1 = (3/2)\hbar\omega$  and  $E_0 = (1/2)\hbar\omega$ , respectively.

amplitude (observed also in the ground state computation; see figure 4). Hence, it lies near that it is caused by the crude iteration scheme we use to find the bandwidths  $h_i$ ; see (32) and (35).

### 3.4 Application to 2d ground states

The Gaussian kernel algorithm defined in section 3.1 is applicable to any number of degrees of freedom  $Nd$ . However, the choices for  $\tilde{Q}^{(i)}$  and  $h_i$  in section 3.2 were constructed for the case  $Nd = 1$ , and hence need to be generalized.

It will be recalled that for  $Nd = 1$  we chose  $\tilde{Q}^{(i)}$  according to (30) because we needed a mechanism to prevent crossing of worlds. However, for  $Nd > 1$  the dynamics is much less constrained—worlds can move so as to exchange positions in configuration space—so that we can be less careful and simply choose

$$\tilde{Q}^{(i)} = Q^{(i)} \quad (36)$$

for  $i = 1, \dots, \tilde{M} = M$ . Note that this prescription is independent of the precise number of degrees of freedom  $Nd$ .

Next, we need to consider an appropriate generalization of constraint (31), to prescribe the width parameters  $h_i$  for a given configuration of worlds

$Q$ . This is most easily effected by finding a suitable replacement for the *a priori* density estimate  $p_i$  in Eq. (31). Any of the general methods in section 2.1 is convenient in this regard, and we will in particular follow the method in section 2.1.2, based on Eq. (21). In order to use (21) we need to specify a subdivision of the configuration space into cells. As mentioned earlier, there are various subdivision methods available, and in our numerical implementation we have chosen the Voronoi subdivision method [24].

In particular, for the configuration space  $\mathbb{R}^{Nd}$  and a configuration of worlds  $Q^{(i)} \in \mathbb{R}^{Nd}$ , the Voronoi cell containing the world  $Q^{(i)}$  is defined by

$$\text{Cell}_i := \left\{ X \in \mathbb{R}^{Nd} : \|X - Q^{(i)}\| < \|X - Q^{(j)}\| \forall j \neq i \right\} \quad (37)$$

We will call  $\text{Cell}_i$  an *inner cell* if it is bounded and an *outer cell* if it is unbounded. By definition the Voronoi cells form a subdivision of configuration space  $\mathbb{R}^{Nd}$ :  $\bigcup_i \overline{\text{Cell}_i} = \mathbb{R}^{Nd}$  and  $\text{Cell}_i \cap \text{Cell}_j = \emptyset$  for  $j \neq i$ . As discussed in section 2, it can be shown that the graph generated by the edges of all Voronoi cells is the dual graph to the one generated by the edges of a Delaunay triangulation (see also figure 1). The

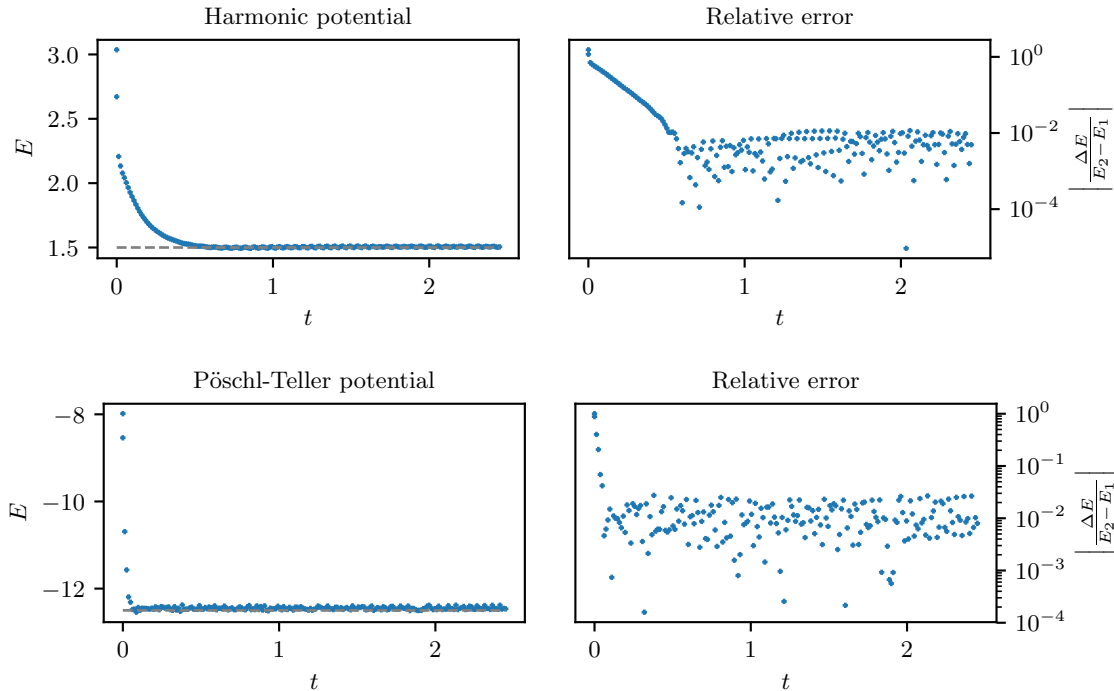


Figure 5: The upper and lower left plots depict the convergence to the first excited state of the harmonic oscillator potential  $V(X) = \frac{1}{2}\hbar^2\omega^2 X^2$  and the Pöschl-Teller potential  $V(X) = \frac{\alpha^2}{2} \frac{\lambda(\lambda+1)}{\cosh^2(\alpha X)}$  for  $\lambda = 6$ , respectively. The energy in the upper plot is plotted in units of  $\hbar\omega$  and for the lower one in units of  $\alpha^2\hbar^2/m$ . For both cases we used an integration time step  $\Delta t = 2.45 \cdot 10^{-5}$  in units of  $\hbar$  and  $10^5$  iterations. Furthermore, the respective relative error is illustrated in the plots on the right and again given in terms difference w.r.t. the first excited state and normalized w.r.t. the energy difference between the first excited and ground state energy, i.e.,  $E_2$  and  $E_1$ . Note that for the harmonic oscillator potential one has  $E_2 = (5/2)\hbar\omega$  and  $E_0 = (3/2)\hbar\omega$ , and for the Pöschl-Teller potential  $E_2 = -8 \cdot \alpha^2\hbar^2/m$  and  $E_1 = -12.5 \cdot \alpha^2\hbar^2/m$ .

Voronoi subdivision is well adapted to our problem of finding an *a priori* density such as (21) from an empirical distribution defined by  $\mathcal{Q}$  as it very naturally incorporates a measure of proximity in configuration space. In accordance with (21), we shall therefore use the corresponding *a priori* density constraint

$$P_h(\tilde{Q}^{(i)}; \mathcal{Q}) \stackrel{!}{=} \frac{1}{M} \frac{1}{|\text{Cell}_i|} =: p_i \quad (38)$$

in place of Eq. (31), to define the widths  $h_i$  for  $Nd > 1$ . Again, the recurrence relation (32) can be employed to quickly obtain an approximate solution.

We have tested this generalized Gaussian kernel algorithm for  $N = 1$  particles and  $d = 2$  spatial dimensions, in two cases: 1) A harmonic potential  $V(X) = \frac{1}{2}\hbar^2\omega^2 X^\top X$  and 2) a Pöschl-Teller type potential. Note that, unlike the harmonic potential, the Pöschl-Teller potential has many more or less natural generalizations in more than one spatial dimension. For our proof of concept study we took the simple choice:  $V(X) = V_1(x_1) + V_1(x_2)$  for  $X = (x_1, x_2)$ ,  $V_1(x) = \frac{\alpha^2}{2} \frac{\lambda(\lambda+1)}{\cosh^2(\alpha x)}$  and  $\lambda = 5$ . The results of the corresponding numerical simulations for  $M = 25$  worlds are shown in figures 6 and 7, respectively, showing convergence to corresponding ground state configurations.

As discussed above, the non-crossing property of worlds is not an issue for  $Nd > 1$ . However, one has to consider a potentially more serious problem concerning the boundary worlds in the outer cells, for which the *a priori* distribution in Eq. (38) reduces to an uninformative value of  $p_i = 0$ , independently of the actual positions of the boundary worlds. In the case  $Nd = 1$  there are only two boundary worlds  $Q^{(1)}$  and  $Q^{(M)}$  whereas, e.g., in our setup for the harmonic potential, with  $Nd = 2$  and  $M = 25$ , we have 16 boundary worlds as depicted in figure 6.

In the case of the harmonic potential the boundary worlds were not found to be problematic, essentially because while their motion is not moderated by other worlds, the strongly-confining nature of the potential does not allow any of the worlds to escape to spatial infinity. In contrast, the Pöschl-Teller potential is asymptotically constant, and hence does not confine the boundary worlds. Due to that fact the corresponding numerical simulation easily becomes unstable. However, a straight-forward solution to circumvent this problem is to introduce additional artificial worlds at fixed positions surrounding the actual worlds  $\mathcal{Q}$ ; see the straight trajectories plotted in figure 7. These artificial boundary worlds act to artificially damp any unwanted oscillations of the outer worlds of  $\mathcal{Q}$  but on the other encode a kind of boundary condition on the Hamiltonian at hand. Hence,

these boundary worlds must be placed at sensible locations, having a sufficient distance to the actual worlds  $\mathcal{Q}$ , so that the accuracy of the world distribution is only changed in regions of configuration space where the density should in any case be very low. One may therefore expect that the accuracy of the numerically inferred moments of observables are not significantly affected. We have not tried to optimize the location of the boundary worlds in our first trial in figure 7, which is why the numerically determined value of the ground state is systematically smaller than the exact one.

These phenomena have to be studied in more detail, however, our analysis already indicates that also in more than one spatial dimension one may expect our proposed approach to be applicable to ground and excited states for various potentials.

## 4 Conclusions

Although there are still several issues to address in order to arrive at a robust integrator for very general settings, we were able to provide a generalization of the MIW algorithm [12], which previously could only treat the case of one particle in one spatial dimension. This generalization was shown to perform well for calculating ground state energies and configurations for the harmonic and Pöschl-Teller potentials, showing good quantitative agreement with the exact solutions in one and two spatial dimensions. We furthermore, demonstrated in one spatial dimension that the proposed algorithm can be adapted to find excited states provided the position of the nodes is known *a priori*. It is very likely that this algorithm can also be generalized in a way that does not assumed the given positions of the nodes but only a given number of them. The corresponding positions of the nodes may then be found by minimizing the energy functional using a gradient descent. It should, however, be emphasized that in more than one spatial dimension the point-like nodes become nodal surfaces, which render the problem of finding excited states more complicated.

Very recently, kernel density estimators have also been applied by Sturniolo, within the framework of the MIW approach, to similarly smooth the empirical density, with numerical calculations made for ground states of harmonic and Lennard-Jones potentials in two and three dimensions [19], using a different method for constructing the estimator, again with promising results. Sturniolo further suggests that exponential kernels may perform better than Gaussian kernels for finding ground state energies, but worse for finding ground state configurations, and that it

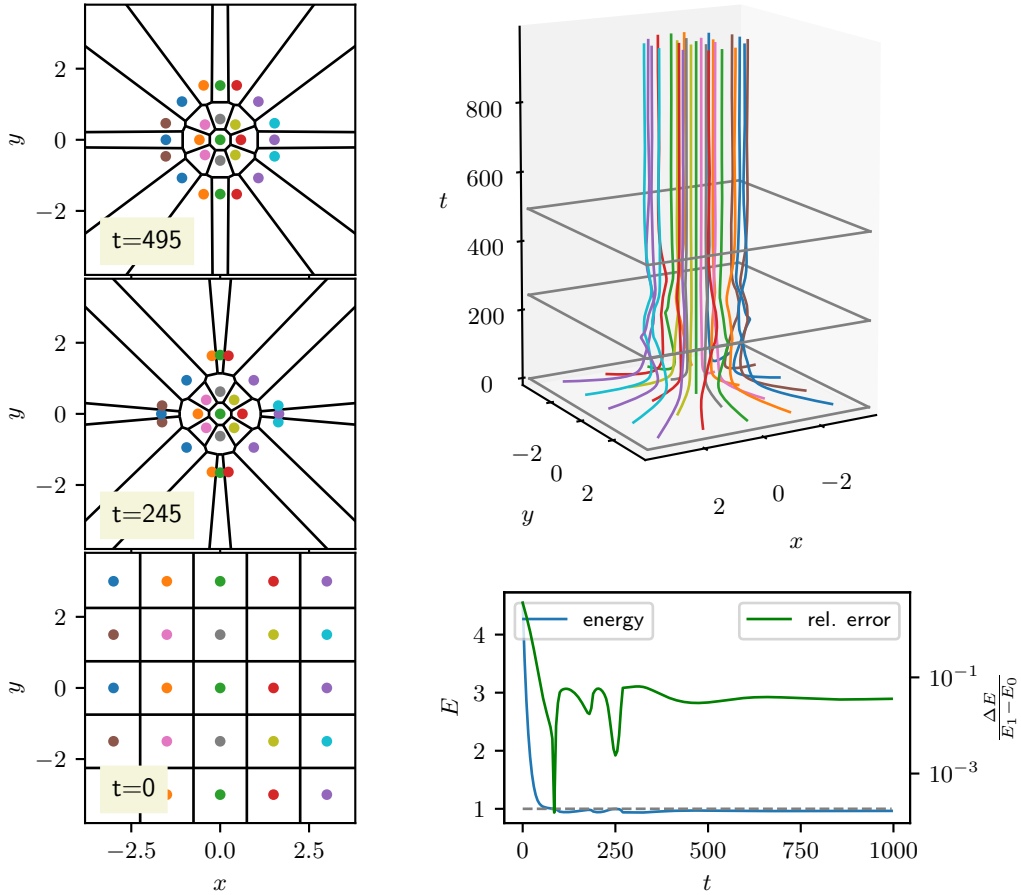


Figure 6: Convergence of the Gaussian kernel algorithm for  $M = 25$  worlds,  $N = 1$  particle, and  $d = 2$  spatial dimensions, in a harmonic potential  $V(X) = \frac{1}{2}\hbar^2\omega^2 X^\top X$ . The plot on the upper right shows the evolution of the configuration of worlds  $\mathcal{Q}$  during the iteration of the algorithm. The integration time step was chosen to be  $\Delta t = 5 \cdot 10^{-2}$  for  $2 \cdot 10^4$  integration steps. The three plots on the left are configuration space snapshots for the respective times  $t$  shown in the lower left corner, respectively. The circles denote the worlds and the black lines illustrate their respective Voronoi cells. The plot in the lower right displays the convergence of the energy, again in units of  $\hbar\omega$ , as well as the relative error. The latter is computed as ratio of the difference of the difference w.r.t. the exact ground state energy (dashed line) and the difference of the exact energies of the first excited and the ground state. Note that in 2d the excited and ground state energies are given by  $E_1 = 2\hbar\omega$ , and  $E_0 = \hbar\omega$ .

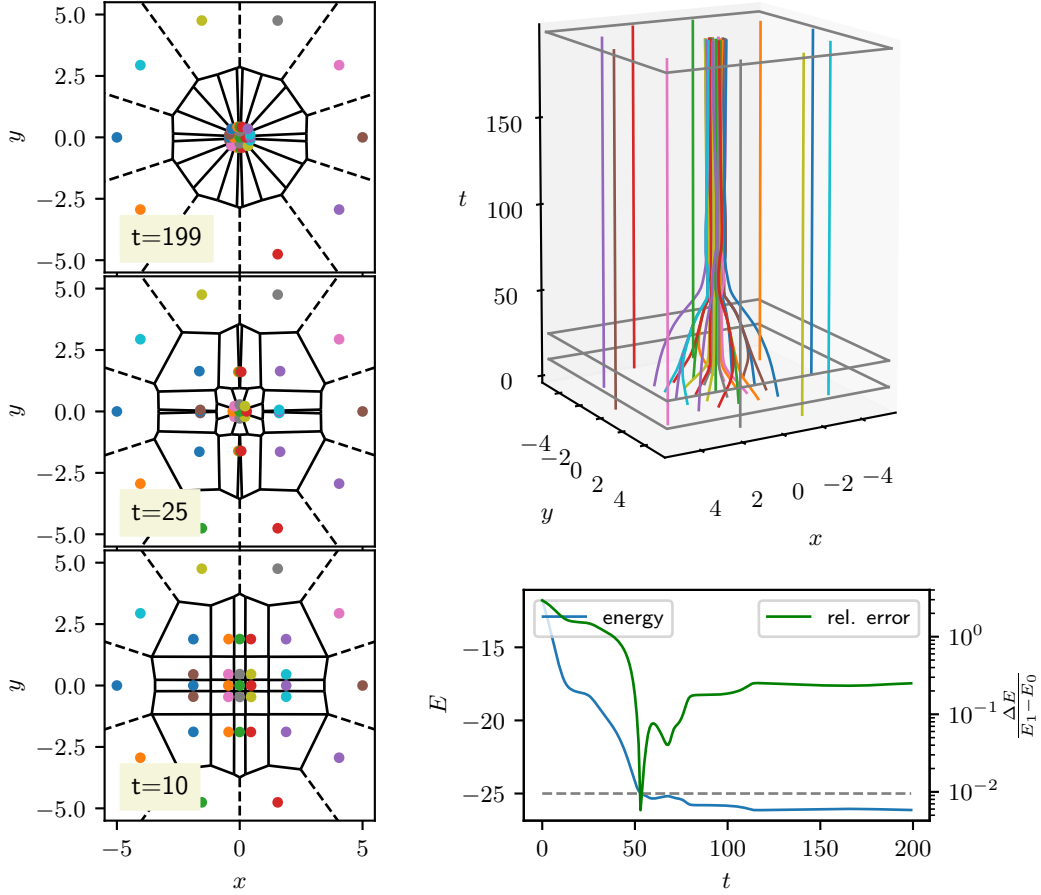


Figure 7: Convergence of the Gaussian kernel algorithm for  $M = 25$  worlds,  $N = 1$  particle, and  $d = 2$  spatial dimensions, in a Pöschl-Teller type potential defined as  $V(X) = V_1(x_1) + V_1(x_2)$  for  $X = (x_1, x_2)$  and  $V_1(x) = \frac{\alpha^2}{2} \frac{\lambda(\lambda+1)}{\cosh^2(\alpha x)}$ , where we chose  $\lambda = 5$ . The plot on the upper right shows the evolution of the configuration of worlds  $\mathcal{Q}$  during the iteration of the algorithm. The integration time step was chosen to be  $\Delta t = 2 \cdot 10^{-2}$  for  $10^4$  integration steps. The three plots on the left are configuration space snapshots for the respective times  $t$  shown in the lower left corner, respectively. The circles denote the worlds and the black lines illustrate their respective Voronoi cells. Note the boundary worlds which, as discussed in the text, have been fixed to lie on a circle of sufficiently large radius to stabilize the iteration. The plot in the lower right displays the convergence of the energy, again in units of  $\alpha^2 \hbar^2 / m$ , as well as the relative error. The latter is computed as ratio of the difference of the difference w.r.t. the exact ground state energy (dashed line) and the difference of the exact energies of the first excited and the ground state. Note that in 2d the excited and ground state energies are given by  $E_1 = -20.5 \cdot \alpha^2 \hbar^2 / m$ , and  $E_0 = -25 \cdot \alpha^2 \hbar^2 / m$ . The computed energy lies systematically below the exact ground state energy. As discussed, this systematic error is caused by the artificially fixed boundary worlds.

may be possible to simulate temperature-dependent tunneling effects in the MIW approach [19].

The original motivation in using the MIW approach in numerical computations was the hope of a generally-applicable method that reduced computational resources as compared to fixed-grid methods. At first sight, the provided numerical implementation still seems to be computationally expensive. Even when neglecting the iteration that determines the bandwidths  $h_i$  in each integration step, see (32), the computational effort scales at least as  $M^2$ , as  $M$  contributions to the potential must be calculated for each world via Eq. (27). There are, however, many tricks to reduce this scaling. Foremost, it has been claimed [23], with respect to kernel density estimation approaches, that in general situation this scaling can be reduced to a linear one in  $M$ . The leading idea behind such an improvement is based on the fact that due to the choice of bandwidths  $h_i$  the Gaussian kernel functions are usually highly peaked in regions where many worlds cluster. Hence, the corresponding kernel functions fall off rapidly and the sum in the density estimator (27) can be truncated. The computational effort to compute values of the exponential function can be reduced further by replacing it with a fixed lookup table that is interpolated according to the scaling introduced by  $h_i$ . Finally, it also has to be emphasized that the iteration to determine the  $h_i$  in (32) usually converges sufficiently after very few iterations, since the configurations of the worlds  $Q$  change only slightly between the integration steps. However, it is also conceivable that the  $h_i$  can be determined dynamically from the world configurations at each time step. Recently ideas were explored in Ref. [25] to determine the bandwidths dynamically, by comparison with dispersion ruled by the heat equation. It seems feasible to obtain similar dynamical laws for the  $h_i$  when the dispersion is ruled by the Schrödinger equation.

The crucial next step should be a systematic study of the  $M$ -dependent scaling of the proposed algorithm given a fixed numerical accuracy that has to be met. Such a study should decide whether the algorithm lives up to the expectation that the exponential scaling of fixed-grid methods can be avoided while maintaining the same numerical accuracy. Thus, we have reasonable confidence that development of our approach in this paper will lead to a general and efficient numerical tool for ground state and other calculations.

**Acknowledgments** We would like to thank M. Ghadimi and T. Gould for valuable discussions. Furthermore, D.-A.D. and H.H. would like to thank Grif-

fith University for its hospitality, while M.J.W.H. and H.M.W. likewise thank the Ludwig Maximilian University. This work was partially funded by the Elite Network of Bavaria through the Junior Research Group “Interaction between Light and Matter” and by FQXi Grant FQXi-RFP-1519.

## References

1. E.H. Lieb, R. Seiringer, J.P. Solovej, and J. Yngvason, *The Mathematics of the Bose Gas and its Condensation*. Oberwolfach Seminars, Vol. 34, Birkhäuser (2005)
2. R. E. Wyatt, *Quantum Dynamics with Trajectories* (Springer, New York, 2005).
3. P. K. Chatteraj, *Quantum Trajectories* (CRC Press, 2010).
4. D.-A. Deckert, D. Dürr, and P. Pickl. *Quantum Dynamics with Bohmian Trajectories*, J. Phys. Chem. A **111**, 10325 (2007).
5. D. Dürr, S. Teufel, *Bohmian Mechanics. The Physics and Mathematics of Quantum Theory.*, Heidelberg. Springer (2009).
6. Sanz, Ángel S., and Salvador Miret-Artés. *Quantum Mechanics with Trajectories*. in A Trajectory Description of Quantum Processes. I. Fundamentals, 187–230. Lecture Notes in Physics. Springer, Berlin, Heidelberg (2012).
7. Benseny, Albert, Guillermo Albareda, Ángel S. Sanz, Jordi Mompart, and Xavier Oriols. *Applied Bohmian Mechanics*. The European Physical Journal D 68 (10):286 (2014).
8. P. Holland, *Computing the Wavefunction from Trajectories: Particle and Wave Pictures in Quantum Mechanics and Their Relation*, Ann. Phys. **315**, 505 (2005).
9. B. Poirier, *Bohmian Mechanics without Pilot Waves*, Chem. Phys. **370**, 4 (2010).
10. G. Parlant, Y.C. Ou, K. Park and B. Poirier, *Classical-Like Trajectory Simulations for Accurate Computation of Quantum Reactive Scattering Probabilities*, Computat. Theoret. Chem. **990**, 3 (2012).
11. J. Schiff and B. Poirier, *Quantum Mechanics without Wavefunctions*, J. Chem. Phys. **136**, 031102 (2012).

12. M. J. W. Hall, D.-A. Deckert, and H. M. Wiseman *Quantum Phenomena Modeled by Interactions between Many Classical Worlds*, Phys. Rev. X 4, 041013 (2014).
13. C. Sebens, *Quantum mechanics as classical physics*, Philosophy of Science Vol. 82, No. 2, pp. 266-291 (2015)
14. K. J. Boström, *Quantum mechanics as a deterministic theory of a continuum of worlds*, Quantum Stud.: Math. Found. 2, 315 (2015).
15. L. Smolin, *Quantum mechanics and the principle of maximal variety*, Found. Phys. 46, 736 (2016).
16. K. Berndl, M. Daumer, D. Dürr, S. Goldstein and N. Zanghì, *A Survey of Bohmian Mechanics*, Il Nuovo Cimento B (1971-1996) **110**, 737 (1995).
17. I. W. McKeague and B. Levin, *Convergence of empirical distributions in an interpretation of quantum mechanics*, Ann. Appl. Probab. **26**, 2540-2555 (2016).
18. H. Herrmann, *Finding stationary states by interacting many worlds*, Master Thesis, Mathematical Institute of the LMU Munich (2016).
19. S. Sturniolo, *Computational applications of the Many Interacting Worlds interpretation of quantum mechanics*, Eprint, arXiv:1709.09880 [quant-ph] (2017).
20. A. J. Izenman, *Review Papers: Recent Developments in Nonparametric Density Estimation*, Journal of the American Statistical Association, 86, 205–224 (1991).
21. W. Scott, *Multivariate density estimation: theory, practice, and visualization*, Hoboken, New Jersey: John Wiley & Sons, Inc, second edition ed. (2015).
22. I. S. Abramson, *On Bandwidth Variation in Kernel Estimates-A Square Root Law*, The Annals of Statistics, 10, 1217–1223 (1982).
23. A. Elgammal, R. Duraiswami, and L. S. Davis, *Efficient Kernel Density Estimation using the Fast Gauss Transform with Applications to Color Modeling and Tracking*, IEEE Transactions on Pattern Analysis and Machine Intelligence, 25, 1499–1504 (2003).
24. J. A. De Loera, J. Rambaau and F. Santos, *Triangulations*, vol. 25 of *Algorithms and Computation in Mathematics* (Springer, Berlin, 2010).
25. Z. I. Botev, J. F. Grotowski and D. P. Kroese, *Kernel density estimation via diffusion*, The Annals of Statistics, Vol. 38, No. 5, 2916–2957, 2010.
26. R. Courant and D. Hilbert, *Methoden der mathematischen Physik*. Springer-Verlag, 1924.
27. A. Ancona, B. Helffer, and T. Hoffmann-Ostenhof, *Nodal domain theorems a la Courant*, Documenta Mathematica, vol. 9, pp. 283–299, 2004.